PAPER

ABA block copolymers comprising a water soluble poly(N-hydroxyethyl acrylamide) B block form self-assemblies of varied morphologies in an aqueous environment†

Alshaimaa Almehmady, Robert Cavanagh, Giuseppe Mantovani* and Snow Stolnik [ID] *

In this study, we apply a combination of SET-LRP and photoinduced LRP techniques to synthesize novel ABA block copolymers comprising poly(N-hydroxyethyl acrylamide) as a water soluble middle B block, flanked by poly(n-butyl acrylate) A blocks: $(n\text{-BA})_m\text{-}b\text{-}(N\text{-HEA})_n\text{-}b\text{-}(n\text{-BA})_m$. NMR analysis of the copolymers in the 'best performing' common solvents indicates the presence of partially solvated poly(n-butyl acrylate) blocks and a well-solvated poly(N-hydroxyethyl acrylamide) block in a DMSO-d_6/acetone-d_6 mixture, whilst the inverse occurs in MeOH-d_4. This partial solvation of the constitutive blocks in the best common solvents may be a contributing factor for the formation of self-assembled structures with varied morphologies and broad particle size distribution on the introduction of a solvent (water) selective for the central poly(N-hydroxyethyl acrylamide) block. With the view of potential biomedical applications, toxicity studies show that the copolymers do not cause appreciable damage to the cell membrane leading to undesirable necrotic cell death, often observed for amphipathic polymeric surfactants, even at relatively high concentrations with 24-hour exposure. We envisage that the middle poly(N-hydroxyethyl acrylamide) block offers the potential to further introduce different surface functionalities, including targeting ligands.

Introduction

Block copolymers self-assemble in a selective solvent and these self-assemblies can assume interesting supramolecular morphologies, including spheres, worms or vesicles. Self-assembly of ABA triblock copolymers in solvents predominantly dissolving their middle B block can bring the A blocks into a core surrounded by the B block forming a loop – a micellar architecture referred to as flower-like micelles in the literature.[1,2] Alternatively, the entropic penalty of such an arrangement of the middle B block may be overcome by the formation of a 'network' structure with 'nodes' of poorly solvated A blocks connected with solvated middle B blocks, leading to the formation of gel-type systems, particularly in a higher concentration regime. AB and ABA block copolymers have been studied for their potential applications in different fields, including biomedical purposes and drug delivery.[3,4] The biomedical applications dictate the nature of the B block to be hydrophilic and water soluble, due to the aqueous nature

of biological environments. Consequently, most explored ABA copolymers in this field include poly(ε-caprolactone)-b-poly(ethylene glycol)-b-poly(ε-caprolactone), poly(N-iso-propylacrylamide)-b-poly(ethylene glycol)-b-poly(N-isopropyl-acrylamide) or poly(L-lactic acid)-b-poly(ethylene glycol)-b-poly(L-lactic acid), whereby the water soluble middle block is typically based on poly(ethylene glycol), with poly(acrylic acid) or poly(isopropylacrylamide) explored in some studies.[5–7] In an interesting study, ABA copolymers were synthesized from cationic amphiphilic polycarbonates, which in a water environment present the cationic B block at the surface of approximately 200–300 nm sized micelles.[8]

Here, we employed poly(N-hydroxyethyl acrylamide) as the water soluble B block, flanked by poly(n-butyl acrylate) as the water insoluble A blocks. To the best of our knowledge, this ABA copolymer structure has not yet been studied. We based the synthesis of $(n\text{-BA})_m\text{-}b\text{-}(N\text{-HEA})_n\text{-}b\text{-}(n\text{-BA})_m$ copolymers on a combination of single electron transfer living radical polymerisation (SET-LRP) and photoinduced living radical polymerisation (FT-LRP) as synthetic methods.[9–11] This approach exploits the principal advantage of SET-LRP to produce a polymer in a fast manner while retaining chain fidelity, if the optimal balance is maintained between initiation and termination, while the synthesis of poly(n-butyl acrylate) blocks uti-

School of Pharmacy, University of Nottingham, Nottingham, NG7 2RD, UK.
E-mail: giuseppe.mantovani@nottingham.ac.uk, snow.stolnik@nottingham.ac.uk

†Electronic supplementary information (ESI) available. See DOI: https://doi.org/10.1039/d3py00615h

lizes previously described conditions for photoinduced living radical polymerisation (FT-LRP).[12]

Common methods for preparing self-assembled systems from block copolymers when these do not directly disperse in a relevant selective solvent, as is the case in the current study, in principle involve mixing of a copolymer solution in a common solvent with a miscible solvent which is selective for one block. In the present study, water represents a selective solvent that preferentially dissolves the poly(N-hydroxyethyl acrylamide) middle A block. We screened a number of solvents and solvent mixtures that are miscible with water to be used as a potential common solvent for $(n\text{-BA})_m\text{-}b\text{-}(N\text{-HEA})_n\text{-}b\text{-}(n\text{-BA})_m$ copolymers, with the data for a DMSO/acetone mixture and methanol as the 'best performers' upon visual inspection presented here. The cytotoxicity of the copolymers was tested in epithelial cells with the view of their potential application at mucosal surfaces. *In vitro* testing focuses on the potential mechanism of toxicity to assess if, due to their amphiphilic architecture similar to amphiphilic surfactants, the copolymers are causing cell membrane damage which normally leads to non-desirable necrotic cell death.

The $(n\text{-BA})_m\text{-}b\text{-}(N\text{-HEA})_n\text{-}b\text{-}(n\text{-BA})_m$ copolymers offer a potential advantage, relative to ABA copolymers with the PEG middle block, of possible further chemistry on the poly(N-hydroxyethyl acrylamide) block by applying *e.g.* orthogonal covalent attachment ('click chemistry') to introduce targeting surface functionalities.

Experimental

Materials

Diethylene glycol bis(2-bromoisobutyrate) (2f-DEBiB), tris[2-(dimethylamino)ethyl]amine (Me₆TREN), propargyl folate and triethylene glycol methacrylate-N₃ (TEGMA-N₃) were synthesised with >98% purity, as described below.

2,2-Bipyridine (bpy, 99%), *N,N*-dimethylformamide (DMF, anhydrous, 99%), copper(I) bromide (Cu(I)Br, 99%), *N*-hydroxyethylacrylamide (*N*-HEA, 97%), dimethylsulfoxide (DMSO, 99%), deuterated solvents like dimethylsulfoxide (DMSO-d_6, 99%), chloroform (CDCl₃, 99%), and acetone (acetone-d_6, 99%) and ethylenediaminetetraacetic acid (EDTA, 99%) were purchased from Sigma-Aldrich. Diethyl ether (Et₂O, 99%) and methanol (MeOH, 99%) were purchased from Fisher Scientific. Copper(II) bromide (Cu(II)Br₂, 99%), copper(I) chloride (Cu(I)Cl, 99%) and *n*-butyl acrylate (*n*-BA, 99%) were purchased from Alfa Aesar. Triethylamine (Et₃N, 99%), formaldehyde aqueous solution (37%), tetrahydrofuran (THF, anhydrous, 99%), tris(2-aminoethyl)amine (99%), 2-bromoisobutyryl bromide (98%), diethylene glycol (99%), folic acid (97%) and propargylamine (98%) were purchased from Sigma-Aldrich. Methacryloyl chloride (97%) was purchased from Alfa Aesar. Petroleum ether (pet. ether, 99%), ethyl acetate (EtOAc, 99%), toluene (99%), dichloromethane (DCM, 99%), acetone (99%), and MgSO₄ were purchased from VWR International.

Methods

Synthesis of (*N*-HEA)ₙ *via* SET-LRP. The procedure was adapted from Simula *et al.*[13] Me₆TREN (4.560 mg, 0.019 mmol) dissolved in deionized water (1.50 mL) was added to a Schlenk tube equipped with a magnetic stir bar, and the tube was sealed with a rubber septum. The solution was bubbled with argon (Ar) for 10 min and left to stir for 10 min. Then, Cu(I)Br (5.68 mg, 0.039 mmol) was added under inert conditions and allowed to disproportionate fully (2 min). A separate clean glass tube was charged with 2f-DEBiB (20 mg, 0.05 mmol), *N*-HEA (205.16 mg, 1.78 mmol), and 2-CEA (26.64 mg, 0.12 mmol) in a mixture of DMSO and DI H₂O (4 : 1 v/v, 2 mL). The mixture was stirred until complete dissolution (typically 5 min); then the solution was bubbled with Ar for 10 min and finally cannulated into the Schlenk tube containing Me₆TREN/Cu⁰–Cuᴵᴵ, previously cooled to 0 °C (t_0). The polymerisation was allowed to proceed at 0 °C under stirring. Purification of the resulting polymer reaction mixture was performed by dialysis, using a wetted dried snake dialysis membrane (cut-off 3.5 kDa) for 5 days against 5 L of water, changing the water every 24 hours. To remove copper from the mixture, EDTA was added to the reaction mixture before dialysis, and the dialysis cycles were carried out *vs.* aqueous EDTA until the disappearance of the green colour from the dialysis bag. For the subsequent cycles, dialysis was performed against DI water. After dialysis, the dialysis tube content was freeze-dried (yield = 200 mg, 79%). Ratio of [2f-DEBiB] : [*N*-HEA] : [2-CEA] : [Cu(I)Br] : [Me₆TREN] = [1] : [36] : [4] : [0.80] : [0.40], target conversion >99%. Quantities used are as follows: 2f-DEBiB (113 mg, 0.28 mmol), Cu(I)Br (32.13 mg, 0.22 mmol), Me₆TREN (25.80 mg, 0.11 mmol) and DMSO : H₂O (4 : 1, 2 mL).

In the further purification step, a copolymer present in DMSO was additionally dialysed against L-cysteine solution for a week, with daily changes of the dialysis medium, with subsequent dialysis against DI water. This was undertaken due to cell toxicity observed in the initial screening of copolymers dialysed against EDTA to remove copper.

Chain extension of (*N*-HEA)ₙ using (*n*-BA)ₘ *via* photoinduced living radical polymerisation. An analogous procedure of chain extension, as the one described above for (*N*-HEAₙ-*co*-(2-CEA)ᵤ), was used here with the following ratios: [Cu(II)Br₂] : [Me₆TREN] = [0.06] : [0.12] w/w, [*n*-BA] : [DMSO] = 1 : 3 v/v. Typical quantities used to target 24 units of *n*-BA (target DP) of (*N*-HEA)₄₀ (MI) are as follows: MI (256 mg, 0.05 mmol), *n*-BA (164.08 mg, 1.28 mmol), Cu(II)Br₂ (1.25 mg, 0.005 mmol), and Me₆TREN (7.741 mg, 0.03 mmol). Depending on the target DP of *n*-BA, the quantities of *n*-BA and DMSO were changed accordingly.

The UV-irradiation source used during photoinduced LRP was a commercially available nail gel curing device (λ_{max} ~ 360 nm) equipped with four 36 W bulbs.

Nuclear magnetic resonance (NMR). The ¹H NMR spectra were recorded on a 400 MHz Bruker DPX400 Ultrashield using deuterated solvents (CDCl₃ and DMSO-d_6). All chemical shifts are reported in parts per million (ppm). Data were elaborated

using MestReNova (Mestrelab, Santiago de Compostela, Spain) software version 6.2.1-7569.

Size exclusion chromatography (SEC). The molecular weight of copolymers was determined by Size Exclusion Chromatography (SEC) using a PL50 system (Polymer Laboratories) equipped with two columns connected in series (Agilent PLgel 5 μm Mixed D, 7.5 × 300 mm) and a refractive index (RI) detector, eluting with DMF + 0.10% LiBr (w/w) at a flow rate of 1 mL min^{-1}. The molecular weights and polydispersity indices of the polymers were calculated according to a calibration curve obtained with PMMA narrow standards (550–2 136 000 g mol^{-1}). Data were elaborated using Cirrus GPC/SEC 3.0 software.

Size exclusion chromatography and multi-angle light scattering (SEC-MALS). The molecular weight of the copolymers was determined by SEC-MALS (in addition to RI-SEC) using a Wyatt Dawn 8 + 1200 infinity series technology. The system has two columns: SEC analytical column for membrane proteins and TSKgel® size exclusion (SW-Type) HPLC column (G3000SWxI, L, 5 μM, 300 Å). The mobile phase used was Dulbecco's phosphate buffered saline (DPBS) with a flow rate of 1 mL min^{-1}. Data were elaborated using ASTRA® software, V.6.1.2.84 (Wyatt Tech Corp).

Attenuated total reflectance-Fourier transform infrared (ATR-FTIR) spectroscopy. Fourier transform infrared spectra were obtained by attenuated total reflectance (ATR) spectrophotometry using a Cary 630 FTIR spectrometer from Agilent Technologies. The instrument was equipped with an ATR diamond single reflection unit. Spectra were acquired in the 4000–650 cm^{-1} range.

Differential scanning calorimetry (DSC). The glass transition temperature (T_g) of the synthesized materials was measured using a TA-Q2000 DSC (TA Instruments) differential scanning calorimeter. The samples were exposed to two cooling–heating cycles in a range from −90 to 250 °C at 10 °C min^{-1} and data from the second cycle are reported. Data were analyzed using the Universal software version 4.5A (see the ESI Fig. S1†).

Formulation by addition of a solvent selective for the poly(N-HEA) block and evaporation. 5.0 mg of the copolymer was dissolved in 10 mL of methanol in a small vial. Under magnetic stirring, 10 mL of deionized water was added dropwise at a flow rate of 1.0 mL min^{-1} using a syringe pump (NE 300, single syringe pump, Just Infusion™, ProSense) at room temperature. Vials were left open overnight in a fume hood to allow for the evaporation of methanol.

Formulation by dialysis against a solvent selective for the poly(N-HEA) block. 5 mg of the copolymer was dissolved in 1 mL of solvent, using either a DMSO/acetone 5 : 1 mixture or methanol, and placed in a wetted snakeskin dialysis tube (cut-off 3.5 kDa). The contents of the dialysis tube were dialyzed against 1 L of deionized water for 3 days, with changes of deionized water every 24 hours.

Particle size analysis by dynamic light scattering (DLS). The particle size and size distribution were measured using a Zetasizer Nano-ZS (Malvern Instruments Ltd) at an angle of 173°, a laser wavelength of 633 nm, and a temperature of 25 °C. Three measurements of each analysed sample were taken and the data were analysed using Malvern software version 7.11.

Morphology characterisation by transmission electron microscopy (TEM). The samples for TEM analysis were prepared by depositing 13 μl of the sample on a carbon-coated copper grid (a Formvar carbon film on a copper 200 hexagonal mesh, FC200HxCu). The samples were allowed to sediment, dried on the grid for 3 hours and then negatively stained by the addition of 13 μl uranyl acetate aqueous solution (3%) for 10 minutes. Excess liquid was removed ('wicked') using filter paper and the samples were examined using an FEI Technai BioTwin-12 system.

Preparation of the samples for cell toxicity testing. The synthesized copolymers were dispersed in DMSO at a concentration of 100 mg mL^{-1} by means of ultrasonication at 37 kHz for 50 minutes. Following sonication, the samples were diluted in Hanks buffered saline solution (HBSS) to achieve a concentration of 1.0 mg mL^{-1} (final DMSO concentration 1.0%). Further serial dilutions were performed in HBSS to produce test concentrations of 1, 5, 20, 100, 200, 500 and 1000 μg mL^{-1}. Sterile 2.5 mL micro-centrifuge tubes were used. The highest DMSO concentration applied *in vitro* was thus 1.0% (v/v), a concentration deemed tolerable in Calu-3 cells.[14] The treatment samples were warmed to 37 °C prior to application on cells.

Cell metabolic activity (MTS) assay. Human lung epithelial Calu-3 cells (supplied by ATCC, passage 35-37) were seeded on clear 96-well plates at a density of 1×10^4 cells per well and cultured for 24 hours in Dulbecco's modified Eagle's medium (DMEM) supplemented with 10% (v/v) of fetal bovine serum (FBS), 0.10 mg mL^{-1} streptomycin, 100 units per mL penicillin, 0.25 μg mL^{-1} amphotericin and 2 mM L-glutamine. On the day of assaying, the culture medium was removed, the cells were washed with phosphate buffered saline (PBS) and the medium in the wells was replaced with 150 μl per well of (n-BA)$_3$-b-(N-HEA)$_{40}$-b-(n-BA)$_3$, (n-BA)$_9$-b-(N-HEA)$_{40}$-b-(n-BA)$_9$, and (n-BA)$_{57}$-b-(N-HEA)$_{40}$-b-(n-BA)$_{57}$ samples (sonicated polymer suspension in buffer) or 1.0% Triton X-100 solution, applied in 1.0% DMSO in HBSS. Following incubation with treatment solutions for 24 hours, the cells were washed with PBS and incubated with 20 μl MTS reagent in 100 μl DMEM per well for 2 hours at 37 °C. The absorbance was read at 492 nm. The relative metabolic activity was normalised with regard to the controls; the vehicle control (1.0% DMSO in HBSS) was taken as 100% metabolic activity, and cells treated with 1.0% Triton X-100 solution (positive control) were set to 0%. Treatments were applied in triplicate and three independent experiments were performed.

Lactate dehydrogenase (LDH) release assay. The cells were treated as described above, and following 24 hour treatment exposure, the LDH release assay (Sigma-Aldrich, TOX7 kit) was performed using the manufacturer's recommended method. This involved removing 50 μl per well of cell-conditioned sample solutions and transferring to a fresh clear 96-well plate. To these solutions, 100 μl per well of LDH reagent was added and the resulting solutions were protected from light by

wrapping the plate with aluminium foil and then incubated for 25 minutes at room temperature. Three wells were used for each concentration (n = 3). Following the incubation step, absorbance was measured at 492 nm. The relative LDH toxicity was calculated by setting the absorbance value of the vehicle control (1.0% v/v DMSO in HBSS) as 0% and the positive control (1.0% Triton X-100) as 100%.

Determination of cellular ROS induction. Intracellular reactive oxygen species (ROS) levels were assessed using the CM-H2DCFDA probe (Thermo Fisher Scientific). The cells were cultured as stated above and exposed to the copolymers applied at their LD_{50} values for 24 hours, as described above. H_2O_2 (1 mM) was used as a positive ROS-inducing control. The cells were then incubated with 10 µM CM-H2DCFDA in HBSS for 30 min at 37 °C. The probe was removed, the cells were washed twice with HBSS and the fluorescence intensity was measured at 490/520 nm (excitation/emission). The measured values were normalized to the vehicle control (set as a value of 1).

Detection of activated caspase-3/7. The CellEvent caspase-3/7 green detection reagent (Thermo Fisher Scientific) was employed to assess the levels of activated caspase-3 and 7. Calu-3 cells were seeded and cultured as described above and following 24 hour exposure to copolymers at their LD_{50} concentrations or 10 µM staurosporine (apoptosis inducing control), 100 µL of 2% (v/v) CellEvent probe diluted in PBS was applied per well for 30 min at 37 °C. Fluorescence intensity was measured at 500/530 nm (excitation/emission) and normalized to the vehicle control (set as a value of 1).

Hoechst/propidium iodide microscopy. Nuclear morphology and permeability were assessed by Hoechst and propidium iodide staining, respectively. Calu-3 cells were seeded in 24 well plates at a density of 6×10^4 cells per well and cultured for 24 hours. The cells were exposed for 24 hours to copolymers applied at their LD_{50} concentrations or 10 µM staurosporine

(positive apoptotic control). Following the exposure, treatments were stopped, the cells were washed with PBS and a cocktail of 1 µM Hoechst 33342 (Thermo Fisher Scientific) and 3 µM propidium iodide (PI; Thermo Fisher Scientific) diluted in PBS was applied for 10 minutes at 37 °C. The staining solution was then removed and the cells were washed with PBS and imaged on an inverted Nikon Eclipse TE 300 fluorescent microscope on DAPI and RFP filters. The images were merged using ImageJ software (v1.52f).

Statistical analysis

The cell response curves for the MTS assays were fitted using a nonlinear normalized response equation through computer-assisted curve fitting with GraphPad Prism software 7.0. This software was also used to carry out statistical analysis. A comparison between groups was performed using one-way ANOVA followed by Tukey's multiple comparison *post hoc* test (N = 3, n = 3).

Results and discussion

The synthesis of the water soluble B block *i.e.* $(N\text{-HEA})_n$ macromolecular initiator was conducted by applying the Single Electron Transfer Living Radical Polymerisation (SET-LRP) technique. This process is based on the phenomenon that in the presence of an aqueous medium, or a binary mixture of water and polar organic solvents (*e.g.* DMSO, THF and alcohols),[15] Cu(I) species tend to disproportionate to produce Cu(0), which then acts as an activator in the SET reaction, and Cu(II)Br$_2$ which, by reacting with radical species, acts as the radical deactivator (Fig. 1). Typically, polydentate ligands, *e.g.* Me$_6$TREN, are required to stabilize the copper species involved in the catalytic cycle.[10] SET-LRP was adopted in this study instead of 'conventional' ARTP, due to its higher ability to maintain the halide chain-end fidelity,[16–20] essential to be able
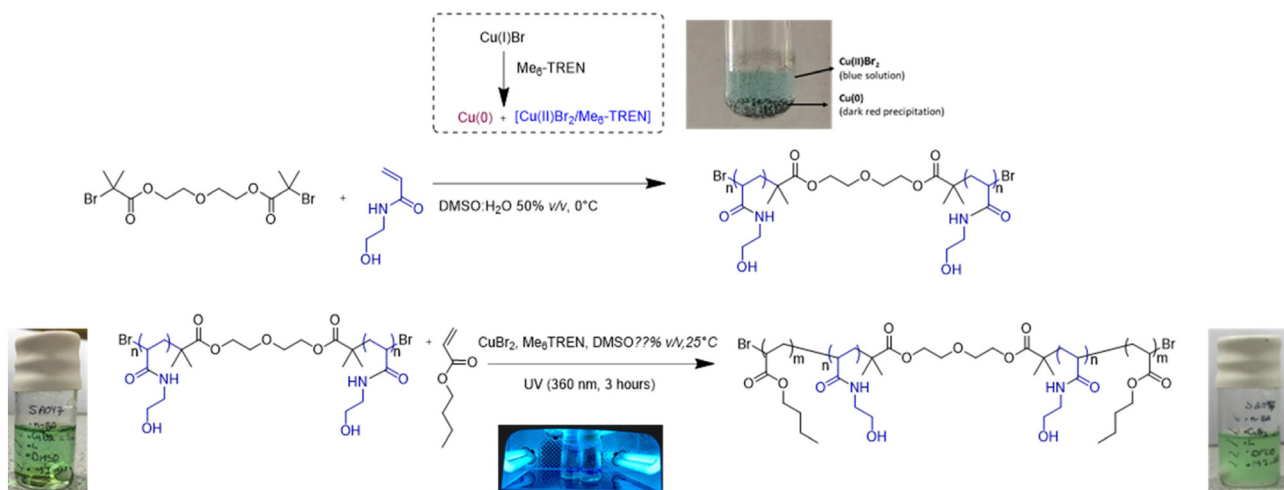

Fig. 1 Schematic of synthesis of ABA $(n\text{-BA})_m\text{-}b\text{-}(N\text{-HEA})_n\text{-}b\text{-}(n\text{-BA})_m$ copolymers. Synthesis of the $(N\text{-HEA})_n$ B block using the macromolecular initiator by single electron transfer-living radical polymerisation (SET-LRP). The growth of $(n\text{-BA})_m$ A blocks by photoinduced LRP using Cu(II)Br$_2$ and Me$_6$TREN as catalyst complexes.

to, in the next stage, extend the hydrophilic B block and generate the desired ABA triblock copolymer structure. This technique has been shown to work more efficiently with monomers such as vinyl chloride,[21] acrylates[22–24] and acrylamides,[25,26] compared to those characterized by lower propagation rates, such as methacrylates. A degree of polymerisation (DP) of 40 was targeted for the $(N\text{-HEA})_n$ macroinitiator with the view to potentially allow the middle block to form a water-solvated loop when the copolymers are present in a water environment.

Data in Fig. 2 show that a near complete $(N\text{-HEA})_n$ conversion was achieved within approximately 30 minutes. Very high $(n\text{-BA})_m$ conversion was also accomplished in all chain extension reactions, yielding polymers with low molecular weight

distributions, although it should be noted that DMF was used as an elution solvent in SEC.

Attributes of the synthesized copolymers are summarized in Table 1. FTIR analysis was applied to confirm the presence of the main functional groups and block composition of the synthesized copolymers[27] (Fig. 3). More specifically, for $(n\text{-BA})_m\text{-}b\text{-}(N\text{-HEA})_{40}\text{-}b\text{-}(n\text{-BA})_m$ copolymers, functional groups are: amide (C=O at 1680–1630 cm^{-1}, stretching, and N–H at 1640–1550 cm^{-1}, bending), ester (C=O at 1750–1730 cm^{-1}, stretching), and alkane (3000–2850 cm^{-1}, stretching). The analysis of FTIR spectra revealed the increased relative intensity of alkane (2875 cm^{-1}, stretching) and ester (1730 cm^{-1} stretching) signals with the increasing length of the poly(n-butyl acrylate) hydrophobic blocks $i.e.$, in order of $(n\text{-BA})_{57}\text{-}b\text{-}(N\text{-HEA})_{40}\text{-}b\text{-}(n\text{-BA})_{57} > (n\text{-BA})_9\text{-}b\text{-}(N\text{-HEA})_{40}\text{-}b\text{-}(n\text{-BA})_9 > (n\text{-BA})_3\text{-}b\text{-}(N\text{-HEA})_{40}\text{-}b\text{-}(n\text{-BA})_3$.

Initially, ^{1}H NMR spectra of $(n\text{-BA})_m\text{-}b\text{-}(N\text{-HEA})_{40}\text{-}b\text{-}(n\text{-BA})_m$ copolymers were obtained in a DMSO-d_6/acetone-d_6 5:1 mixture (Fig. 4). The addition of a less polar solvent, acetone-d_6, to DMSO-d_6 was aimed to promote solvation of more hydrophobic $(n\text{-BA})_m$ blocks (E_T^N 0.356 and 0.460 for acetone and DMSO, respectively).[29] This was based on the observation during copolymer synthesis that the starting macroinitiator, $(N\text{-HEA})_{40}$, dissolves initially in DMSO as a clear solution, but the reaction mixture becomes gradually turbid, $i.e.$, indicating decreased solubility, with the growth of
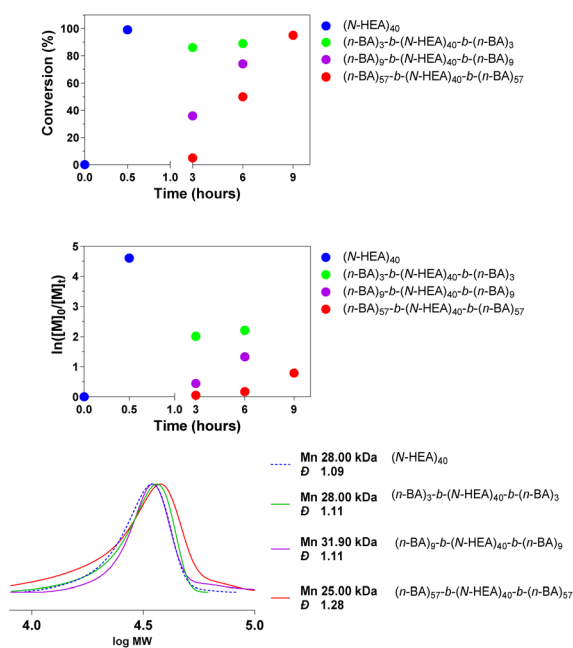
Fig. 2 Conversion to $(n\text{-BA})_m\text{-}b\text{-}(N\text{-HEA})_{40}\text{-}b\text{-}(n\text{-BA})_m$ copolymers of the precursor $(N\text{-HEA})_{40}$ (top). SEC trace of the synthesized copolymers recorded in DMF (with LiBr 1%) (bottom).
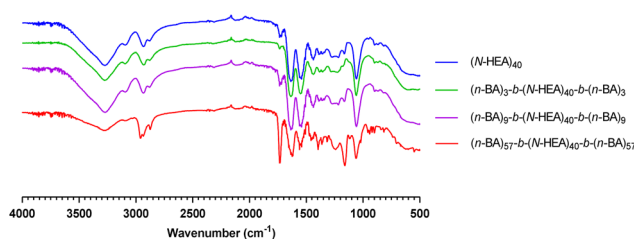
Fig. 3 FTIR spectra of the synthesized $(n\text{-BA})_m\text{-}b\text{-}(N\text{-HEA})_{40}\text{-}b\text{-}(n\text{-BA})_m$ copolymers and starting $(N\text{-HEA})_{40}$ macroinitiator. The copolymers demonstrated similar transmittance, apart from $(n\text{-BA})_{57}\text{-}b\text{-}(N\text{-HEA})_{40}\text{-}b\text{-}(n\text{-BA})_{57}$, $(M_{n,theo}$ 19.60 kDa), which shows stronger transmittance in the ester region (C=O at 1750–1730 cm^{-1}, stretching).

Table 1 Molecular attributes of $(n\text{-BA})_m\text{-}b\text{-}(N\text{-EA})_{40}\text{-}b\text{-}(n\text{-BA})_m$ copolymers synthesized from the hydrophilic macroinitiator $(N\text{-HEA})_{40}$

Composition[a]	t.DP[b] [M]	Conv[c] (%)	$M_{n(theo)}$[d] (kDa)	(BA)$_m$: $(N\text{-HEA})_x$: (BA)$_m$ ratio	M_n (^{1}H NMR)[f] (kDa)	M_n (GPC)[e] (kDa)	Đ[e]
$(N\text{-HEA})_{40}$ initiator	40	>99	5.00	1.0[f]	10.00	28.40	1.09
$(n\text{-BA})_3\text{-}b\text{-}(N\text{-HEA})_{40}\text{-}b\text{-}(n\text{-BA})_3$	10	89	6.50	0.11 : 1.0 : 0.11[f]	12.40	28.20	1.11
$(n\text{-BA})_9\text{-}b\text{-}(N\text{-HEA})_{40}\text{-}b\text{-}(n\text{-BA})_9$	24	76	8.40	0.5 : 1.0 : 0.5[g]	73.00	31.80	1.11
$(n\text{-BA})_{57}\text{-}b\text{-}(N\text{-HEA})_{40}\text{-}b\text{-}(n\text{-BA})_{57}$	120	95	19.60	1.57 : 1.0 : 1.57[f]	51.00	25.20	1.28

[a] Number of units in each block of the ABA copolymer was calculated (t.DP × fractional conversion calculated by ^{1}H NMR) assuming 100% initiator efficiency.[28] [b] t.DP is the target degree of polymerisation relative to initiator [2f-DBiB] $i.e.$, targeted number of monomeric units (M). [c] Conv (%) is the percent of the monomer converted to the polymer, calculated by ^{1}H NMR. [d] $M_{n\ theo}$ is the theoretical number-average molecular weight calculated as follows = [((t.DP of $M \times M_{wt}$ of monomer) × fractional conversion] + 404.10 g mol^{-1}. [e] Determined by SEC using DMF as the eluent (+1% LiBr). The system was calibrated using a PMMA standard. [f] Calculated from ^{1}H NMR of the (co)polymer in MeOH-d_4. [g] Calculated from ^{1}H NMR of the (co)polymer in a mixture of DMSO-d_6/CDCl$_3$.
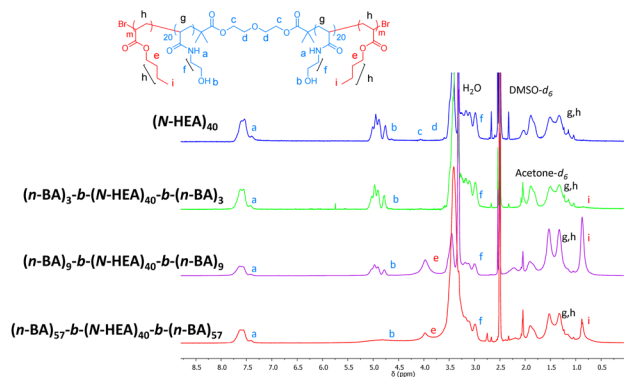
Fig. 4 ^{1}H NMR spectra of the synthesized $(n\text{-BA})_m$-b-$(N\text{-HEA})_{40}$-b-$(n\text{-BA})_m$ copolymers in the DMSO-d_6/acetone-d_6 mixture. Spectrum of the $(N\text{-HEA})_{40}$ macroinitiator recorded in DMSO-d_6 and spectra of the copolymers in the DMSO-d_6/acetone-d_6 mixture at a ratio of 5 : 1 v/v.

Fig. 5 ^{1}H NMR spectra of the synthesized $(n\text{-BA})_m$-b-$(N\text{-HEA})_{40}$-b-$(n\text{-BA})_m$ copolymers and starting $(N\text{-HEA})_{40}$ macroinitiator recorded in MeOH-d_4. Concentration 3 mg/0.6 ml w/v.

$(n\text{-BA})_m$ blocks (as illustrated by the image on the right in Fig. 1). As shown in Fig. 4, the distinguished signals for $(N\text{-HEA})_{40}$ are $-NH$ and $-OH$ (labelled a and b), appearing as broad peaks at ~7.75–7.35 ppm and ~5.13–4.70 ppm, respectively. For the $(n\text{-BA})_m$ moiety, prominent signals observed are $-COOCH_2$ and $-CH_2CH_3$ as broad peaks at ~4.20–3.75 ppm and ~0.95–0.70 ppm, respectively. Regarding copolymers, $(n\text{-BA})_3$-b-$(N\text{-HEA})_{40}$-b-$(n\text{-BA})_3$ shows a small $-CH_2CH_3$ peak with the absence of an ester peak at 3.75 ppm, which might be due to the relatively short $(n\text{-BA})_3$ block length. The $(n\text{-BA})_9$-b-$(N\text{-HEA})_{40}$-b-$(n\text{-BA})_9$ spectrum, on the other hand, reveals both $-OH$ peaks at ~5.13–4.70 ppm of $(N\text{-HEA})_{40}$, as well as a broad peak at ~3.75 ppm which resonates for $(n\text{-BA})_m$ ester $(-COOCH_2)$, with a high broad peak at ~0.70 ppm for the $(n\text{-BA})_m$ methyl group $(-CH_2CH_3)$. For the $(n\text{-BA})_{57}$-b-$(N\text{-HEA})_{40}$-b-$(n\text{-BA})_{57}$ copolymer, smaller peaks were observed for $(n\text{-BA})_m$ ester $(-COOCH_2)$ and methyl $(-CH_2CH_3)$ groups, presumably due to the vicinity of a large peak of water which might be present due to the hygroscopicity of DMSO.

Fig. 4 further shows the differences in the NMR spectra for $(n\text{-BA})_9$-b-$(N\text{-HEA})_{40}$-b-$(n\text{-BA})_9$ and $(n\text{-BA})_{57}$-b-$(N\text{-HEA})_{40}$-b-$(n\text{-BA})_{57}$ copolymers when present in a relatively polar DMSO-d_6/acetone-d_6 solvent mixture. For $(n\text{-BA})_9$-b-$(N\text{-HEA})_{40}$-b-$(n\text{-BA})_9$, peaks for both structural components, $-(N\text{-HEA})$ and $(n\text{-BA})$, are distinguishable in the spectrum, indicating that they are, to some extent, solvated and, if the copolymer forms some supramolecular structures, both structural components are fairly solvated.

In the case of the $(n\text{-BA})_{57}$-b-$(N\text{-HEA})_{40}$-b-$(n\text{-BA})_{57}$ copolymer, an $(N\text{-HEA})$ relevant $p\text{-}NH$ peak at ~7.75–7.35 ppm is present in the spectrum, while peaks at ~5.13–4.70 ppm for $-OH$ and $(n\text{-BA})_m$ relevant ester $(-COOCH_2)$ peak at ~4.20–3.75 ppm both appear obstructed. An $(n\text{-BA})_m$ relevant $-CH_2CH_3$ peak at ~0.95–0.70 ppm is significantly reduced, relative to $(n\text{-BA})_9$-b-$(N\text{-HEA})_{40}$-b-$(n\text{-BA})_9$, despite substantially larger $(n\text{-BA})$ blocks. The latter would indicate that, with an increase in their size, the $(n\text{-BA})_m$ blocks are less solvated in the DMSO-d_6/acetone-d_6 mixture pointing to the presence of the copolymer structure
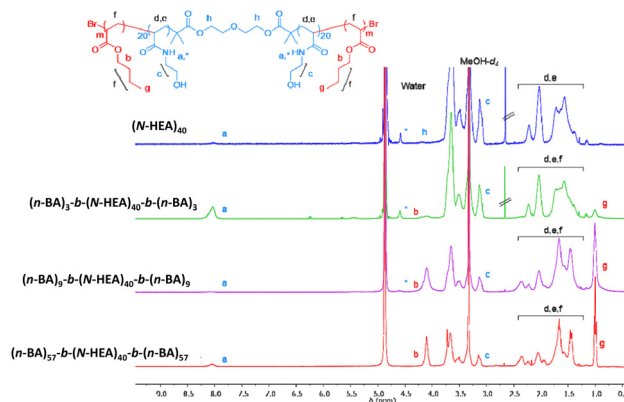
where $(n\text{-BA})_{57}$ end-chains are forming a less solvated regions in the presence of more solvated $(N\text{-HEA})_{40}$ moieties.

^{1}H NMR spectra were also recorded in MeOH-d_4 (Fig. 5). In these spectra, the amide peak $(-NH, \delta\ 7.90\ \text{ppm})$ of the hydrophilic $(N\text{-HEA})_{40}$ macroinitiator appears smaller than expected. Moreover, hydroxyl $-OH$ groups are not visible in the spectrum, likely attributable to deuterium exchange with MeOH-d_4.

An interesting peak was observed at ~4.50 ppm, which might be referred to as either another shift of the amide peak $(-NH)$ of $(N\text{-HEA})_{40}$, or resonance of hydrogen bonding between solvent molecules and amide.[28–30] This small peak is present in $(n\text{-BA})_3$-b-$(N\text{-HEA})_{40}$-b-$(n\text{-BA})_3$ and $(n\text{-BA})_9$-b-$(N\text{-HEA})_{40}$-b-$(n\text{-BA})_9$, but not in $(n\text{-BA})_{57}$-b-$(N\text{-HEA})_{40}$-b-$(n\text{-BA})_{57}$. This corroborates with the observation of increased intensity in the ester peak $(-COOCH_2, \delta \sim 4.00\ \text{ppm})$ and methyl group $(-CH_2CH_3, \delta\ 0.90\ \text{ppm})$ as $(n\text{-BA})_m$ blocks increase in length. This would indicate that in MeOH-d_4, a solvent preferential for $(n\text{-BA})_m$, these solvated blocks might be masking $(N\text{-HEA})_{40}$ from interaction with the MeOH-d_4 solvent. In other words, with an increase in n-BA blocks, the structures formed in MeOH-d_4 may comprise well-solvated flank $(n\text{-BA})_m$ blocks and partially solvated $(N\text{-HEA})_{40}$ areas, the structure inverse to the situation in the DMSO-d_6/acetone-d_6 mixture.

As ^{1}H NMR analyses in both solvent media used (DMSO-d_6/acetone-d_6 mixture in Fig. 4 and MeOH-d_4 in Fig. 5) reveal the evidence of incomplete solvation of $(N\text{-HEA})_{40}$ or $(n\text{-BA})_m$ copolymer blocks, the actual degree of polymerisation for each block was calculated from monomer conversion (Table 1).

The analysis of the glass transition temperature, T_g, of the copolymers is summarized in Fig. 6. A T_g value of 123.23 °C was determined for the starting macroinitiator, $(N\text{-HEA})_{40}$, and indicates that, at approximately room temperatures, the $(N\text{-HEA})_{40}$ chain motion is restricted, $i.e.$, the material is glassy. Conversely, T_g values for poly(n-butyl acrylate) homopolymers, $(n\text{-BA})_{12}$ and $(n\text{-BA})_{60}$, were determined to be −52.89 °C and −50.36 °C, respectively, which is consistent with previous reports.[31] These T_g values indicate that under experimental
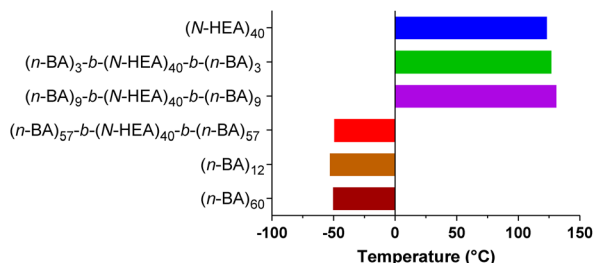
Fig. 6 Glass transition temperature (T_g) of the synthesized $(n\text{-BA})_m\text{-}b\text{-}(N\text{-HEA})_{40}\text{-}b\text{-}(n\text{-BA})_m$ copolymers. Comparisons were made with poly(hydroxy acrylamide) and poly(butyl acrylate) homopolymers.

Fig. 7 Hydrodynamic particle size distribution profiles for the self-assembled structure formed from $(n\text{-BA})_3\text{-}b\text{-}(N\text{-HEA})_{40}\text{-}b\text{-}(n\text{-BA})_3$, $(n\text{-BA})_9\text{-}b\text{-}(N\text{-HEA})_{40}\text{-}b\text{-}(n\text{-BA})_9$ and $(n\text{-BA})_{57}\text{-}b\text{-}(N\text{-HEA})_{40}\text{-}b\text{-}(n\text{-BA})_{57}$ copolymers by applying different protocols. Protocols are addition of the $(N\text{-HEA})_{40}$ selective solvent (water) to the copolymer in methanol, followed by evaporation (graphs in the left column); dialysis of the copolymer in methanol against water as the $(N\text{-HEA})_{40}$ selective solvent (middle column), and dialysis of the copolymer in a DMSO/acetone mixture against the $(N\text{-HEA})_{40}$ selective solvent (right column). Data show particle size distribution (intensity) profiles from dynamic light scattering measurements for one batch per protocol. PDI is the polydispersity index. Concentration of polymers in MetOH and the DMSO/acetone 5 : 1 mixture at 0.5 mg mL^{-1}.

conditions close to room temperature, $(n\text{-BA})_m$ chains are mobile and the material is rubber in nature.

Regarding ABA copolymers, T_g for $(n\text{-BA})_3\text{-}b\text{-}(N\text{-HEA})_{40}\text{-}b\text{-}(n\text{-}$ $\text{BA})_3$ and $(n\text{-BA})_9\text{-}b\text{-}(N\text{-HEA})_{40}\text{-}b\text{-}(n\text{-BA})_9$ are at 126.9 °C and 131.0 °C, respectively, values close to T_g at 123.23 °C for the starting $(N\text{-HEA})_{40}$ macroinitiator. This would indicate that, in a dry state, the chain motion of these copolymers is restricted and that their behaviour is predominantly influenced by the $(N\text{-HEA})_{40}$ block. Inversely, $(n\text{-BA})_{57}\text{-}b\text{-}(N\text{-HEA})_{40}\text{-}b\text{-}(n\text{-BA})_{57}$, the copolymer with the $(n\text{-BA})_m$ blocks larger than $(N\text{-HEA})_{40}$ ($M_{n,theo}$ 14.6 kDa *vs.* 5.0 kDa, respectively), has a T_g of −49.38 °C, which is closer to that of $(n\text{-BA})_{60}$ at −50.36 °C. This might indicate that the copolymer chains are relatively mobile at room temperature, *i.e.*, copolymer behaviour is dominated by the $(n\text{-BA})_{57}$ blocks, important information for storage conditions of potential drug delivery systems based on these copolymers.

It should be noticed that only one glass transition peak was observed in DSC thermograms for the $(n\text{-BA})_m\text{-}b\text{-}(N\text{-HEA})_n\text{-}b\text{-}(n\text{-}$ $\text{BA})_m$ copolymers, including $(n\text{-BA})_{57}\text{-}b\text{-}(N\text{-HEA})_{40}\text{-}b\text{-}(n\text{-BA})_{57}$ (ESI, Fig. S1†). This would indicate that the poly(n-BA) and poly(N-HEA) moieties in these copolymers are miscible in the dry state. A similar observation was observed for $(n\text{-BA})_m\text{-}g\text{-}$ polystyrene copolymer series where with an increase in the number of grafted polystyrene chains, the T_g of $(n\text{-BA})_m$ was increased.[32] By comparing the T_g values of $(n\text{-BA})_3\text{-}b\text{-}(N\text{-HEA})_{40}\text{-}$ $b\text{-}(n\text{-BA})_3$, $(n\text{-BA})_9\text{-}b\text{-}(N\text{-HEA})_{40}\text{-}b\text{-}(n\text{-BA})_9$ and $(n\text{-BA})_{57}\text{-}b\text{-}(N\text{-}$ $\text{HEA})_{40}\text{-}b\text{-}(n\text{-BA})_{57}$ at 123.23, 126.96 and −49.38 °C, respectively, a clear relationship emerges between the length of the poly(n-BA) blocks and T_g, whereby as the $(n\text{-BA})_m$ block length is increased, the glass-transition temperature shifts towards its glass-transition temperature indicating that $(n\text{-BA})_{57}\text{-}b\text{-}(N\text{-}$ $\text{HEA})_{40}\text{-}b\text{-}(n\text{-BA})_{57}$ would show soft and elastic behaviour at room temperature.

Fig. 7 shows hydrodynamic particle size distribution profiles for $(n\text{-BA})_m\text{-}b\text{-}(N\text{-HEA})_{40}\text{-}b\text{-}(n\text{-BA})_m$ copolymer assemblies obtained by different protocols; addition of a solvent selective for the B block (water) into the copolymer present in methanol solvent, or dialysis of copolymers from either methanol or the DMSO : acetone mixture against the solvent selective for the B block (water). The profiles, in general, show the average particle size in the 250–450 nm range, with relatively broad par-
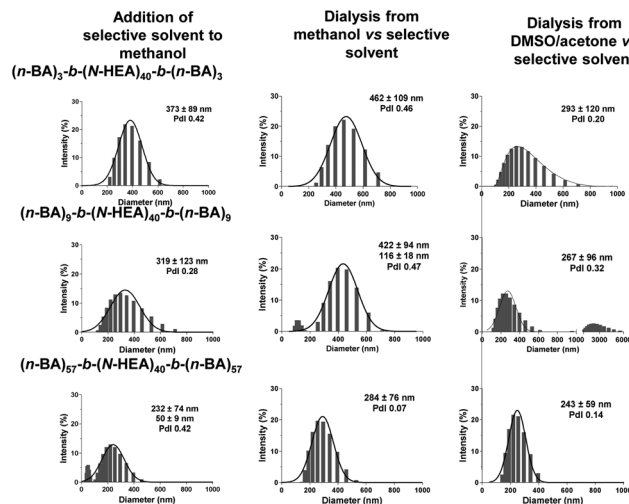
ticle size distributions and high polydispersities. Inspecting the distribution profiles obtained, it is difficult to distinguish possible trends and impacts on the particle size distribution of either a formulation protocol of selective solvent introduction, common solvent quality, *i.e.*, the use of methanol or the DMSO/acetone mixture, or different copolymer compositions. It, however, appears that the $(n\text{-BA})_{57}\text{-}b\text{-}(N\text{-HEA})_{40}\text{-}b\text{-}(n\text{-BA})_{57}$ copolymer forms smaller self-assemblies, relative to other copolymers tested. Referring here to ^{1}H NMR spectra in MeOH-d_4 (Fig. 5), where the structures formed comprise well-solvated $(n\text{-BA})_m$ blocks and partially solvated $(N\text{-HEA})_{40}$ blocks, the assembly reorganization would need to occur on the addition of a solvent (water) selective for (N-HEA) blocks, which differs from the scenario where copolymers in the DMSO-d_6/acetone-d_6 mixture form a less solvated core of $(n\text{-BA})_m$ blocks in the presence of more solvated $(N\text{-HEA})_{40}$ blocks; the latter structure would not need to undergo reorganization on water addition.

The morphologies of $(n\text{-BA})_m\text{-}b\text{-}(N\text{-HEA})_{40}\text{-}b\text{-}(n\text{-BA})_m$ self-assembled structures assessed by transmission electron microscopy (TEM) are presented in Fig. 8. The images depict different morphologies and point to their dependence on both, the copolymer composition and assembly protocol. For example, for the $(n\text{-BA})_3\text{-}b\text{-}(N\text{-HEA})_{40}\text{-}b\text{-}(n\text{-BA})_3$ copolymer present in methanol, the addition of water as the solvent selective for the central $(N\text{-HEA})_{40}$ block resulted in clusters of dis-
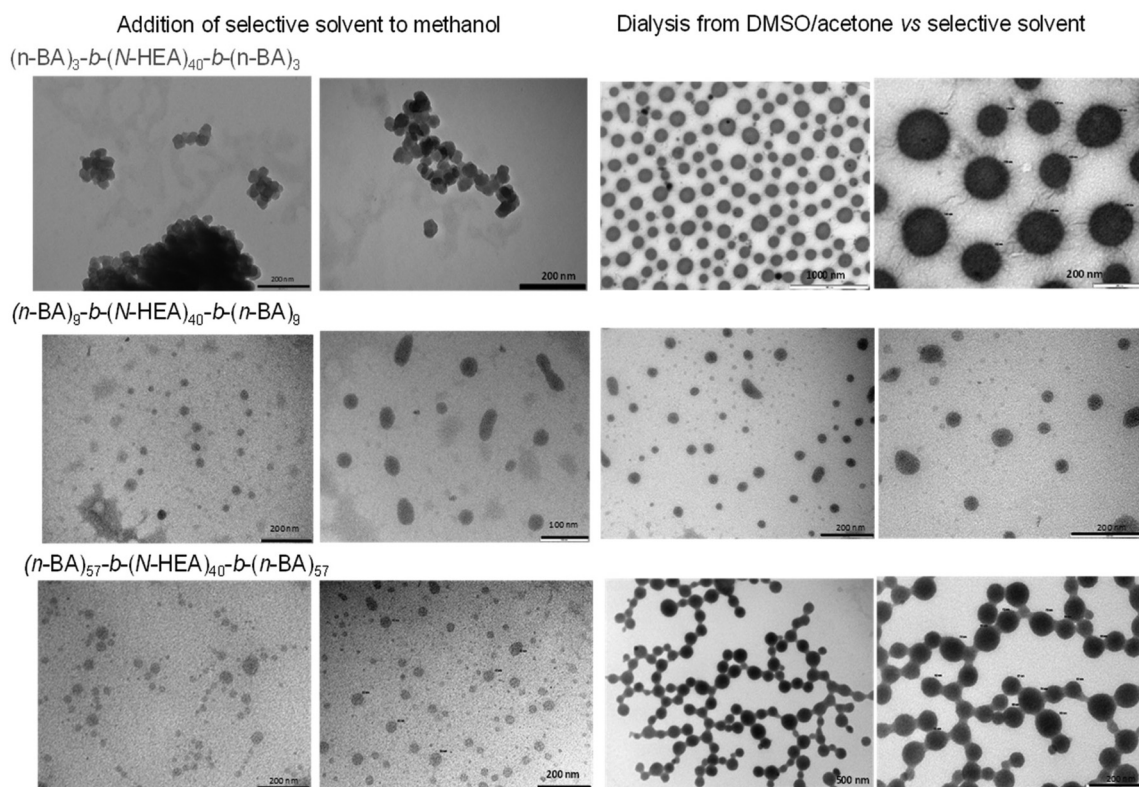
Addition of selective solvent to methanol   Dialysis from DMSO/acetone *vs* selective solvent

$(n\text{-}BA)_3\text{-}b\text{-}(N\text{-}HEA)_{40}\text{-}b\text{-}(n\text{-}BA)_3$

$(n\text{-}BA)_9\text{-}b\text{-}(N\text{-}HEA)_{40}\text{-}b\text{-}(n\text{-}BA)_9$

$(n\text{-}BA)_{57}\text{-}b\text{-}(N\text{-}HEA)_{40}\text{-}b\text{-}(n\text{-}BA)_{57}$

Fig. 8 Transmission electron microscopy (TEM) images of self-assembled structures formed from $(n\text{-}BA)_3\text{-}b\text{-}(N\text{-}HEA)_{40}\text{-}b\text{-}(n\text{-}BA)_3$, $(n\text{-}BA)_9\text{-}b\text{-}(N\text{-}HEA)_{40}\text{-}b\text{-}(n\text{-}BA)_9$ and $(n\text{-}BA)_{57}\text{-}b\text{-}(N\text{-}HEA)_{40}\text{-}b\text{-}(n\text{-}BA)_{57}$ copolymers by applying different protocols. Protocols are addition of water as the $(N\text{-}HEA)_{40}$ selective solvent to copolymers in methanol followed by evaporation (images in left two columns), and dialysis of copolymers in a DMSO/acetone 5 : 1 mixture against the $(N\text{-}HEA)_{40}$ selective solvent (images in right two columns). Images at different magnifications (as indicated in the scale bar) and different fields of view are shown.

crete but irregular (somewhat angular) species around 40–50 nm in size, while its dialysis from the DMSO/acetone mixture against water produced discrete, spherical species of approximately 50–200 nm in size with interesting 'hairy protrusions'. The $(n\text{-}BA)_9\text{-}b\text{-}(N\text{-}HEA)_{40}\text{-}b\text{-}(n\text{-}BA)_9$ copolymer produced a significant population of elongated self-assemblies around 30–40 nm in size, not observed for other copolymers; the $(n\text{-}BA)_{57}\text{-}b\text{-}(N\text{-}HEA)_{40}\text{-}b\text{-}(n\text{-}BA)_{57}$ copolymer produced around 40–50 nm sized assemblies regardless of the protocol, but in the case of dialysis from the DMSO/acetone protocol, these appear to be connected with 'thick bridges' between individual species. Considering the latter observation, TEM images were taken on 'dried samples' prepared at room temperature. Taking into account the DSC data (Fig. 6), in their dry state, the copolymers will possess different chain mobilities, with $(n\text{-}BA)_{57}\text{-}b\text{-}(N\text{-}HEA)_{40}\text{-}b\text{-}(n\text{-}BA)_{57}$ copolymer behaviour dominated by relatively mobile chains of $(n\text{-}BA)_{57}$ blocks (T_g −49.38 °C). This may result in a formation of the observed 'thick bridges' (Fig. 8) during TEM sample preparation, however, it does not provide an explanation for differences in the morphologies of $(n\text{-}BA)_{57}\text{-}b\text{-}(N\text{-}HEA)_{40}\text{-}b\text{-}(n\text{-}BA)_{57}$ self-assemblies formed by two different protocols. In contrast, one would not expect changes in the morphology of $(n\text{-}BA)_3\text{-}b\text{-}(N\text{-}HEA)_{40}\text{-}b\text{-}(n\text{-}BA)_3$ and $(n\text{-}BA)_9\text{-}b\text{-}(N\text{-}HEA)_{40}\text{-}b\text{-}(n\text{-}BA)_9$ assemblies during

TEM sample preparation due to a dominant effect of high T_g of the $(N\text{-}HEA)_{40}$ block in these copolymers (Fig. 6).

We observed profound discrepancies in particle size analysis obtained from dynamic light scattering (Fig. 7) and particle sizes seen in TEM microscopy images (Fig. 8). At this stage, it is not clear what may be the reason(s) for this. For some cases, one may suggest that this might be due to the presence of aggregated or 'bridged' polymeric self-assemblies, *e.g.* for $(n\text{-}BA)_3\text{-}b\text{-}(N\text{-}HEA)_{40}\text{-}b\text{-}(n\text{-}BA)_3$ formed from methanol on the addition of the selective solvent, or for $(n\text{-}BA)_{57}\text{-}b\text{-}(N\text{-}HEA)_{40}\text{-}b\text{-}(n\text{-}BA)_{57}$ formed by dialysis against the selective solvent; however, this does not provide an appropriate explanation for all the studied systems.

Observations in NMR spectra (Fig. 4 and 5) may contribute to the discussion on morphologies and particle size of $(n\text{-}BA)_m\text{-}b\text{-}(N\text{-}HEA)_{40}\text{-}b\text{-}(n\text{-}BA)_m$ self-assemblies. The NMR spectra were recorded in the same common solvents as used in the self-assembly formation, and indicate that in the two common solvent systems used (DMSO/acetone and methanol; selected as the 'best performing' in visual observations of solubility) 'pre-assembled' structures exist even prior to the addition of a solvent selective for the $(N\text{-}HEA)_{40}$ middle B block. The structures of these 'pre-assemblies' could remain relatively unchanged during the introduction in the selective

solvent in the case when DMSO/acetone is used as a common solvent in which copolymer chains form well-solvated (N-HEA)$_{40}$ and poorly solvated (n-BA)$_m$ regions. Alternatively, they need to undergo structural reorganisation on the introduction of the selective solvent for (N-HEA)$_{40}$ to copolymers initially present in methanol where solvated (n-BA)$_m$ and poorly solvated (N-HEA)$_{40}$ regions are present.[33] Furthermore, one needs to consider the tendency of block copolymers to

become kinetically trapped in non-equilibrium states, meaning that the structures they adopt depend on the processing route taken,[34] as it would be the case in this study (Fig. 8).

It should be noted that the addition of a solvent preferential for the (N-HEA)$_{40}$ B-block into copolymers present in a common solvent in all cases resulted in the formation of particulate self-assemblies, rather than hydrophobic blocks forming interconnected domains separated by a hydrophilic B block that could result in the formation of a gel structure. This would indicate that for (n-BA)$_m$-b-(N-HEA)$_{40}$-b-(n-BA)$_m$ ABA copolymers, the concentrations used in their self-assembly process are relatively low, resulting in isolated particles, where the two hydrophobic A-blocks preferentially reside in the core, and the mid B-block will create a hydrophilic surface,[33] as would also be indicated from the observed colloidal stability of their suspensions to aggregation.

In further analysis of the synthesized materials, the cellular toxicity of (n-BA)$_m$-b-(N-HEA)$_{40}$-b-(n-BA)$_m$ copolymers was initially assessed by applying LDH release and MTS assays to evaluate cell membrane integrity and cellular metabolic activity, respectively. The data in Fig. 9 illustrate that on 24 hour exposure, the applied copolymers did not cause statistically significant damage to the cell plasma membrane that would lead to the release of intracellular LDH enzymes. The metabolic MTS assay demonstrates that the exposure to the copolymers results in molecular structure-dependent cellular toxicity, with relatively high calculated 50% lethal dose (LD$_{50}$)
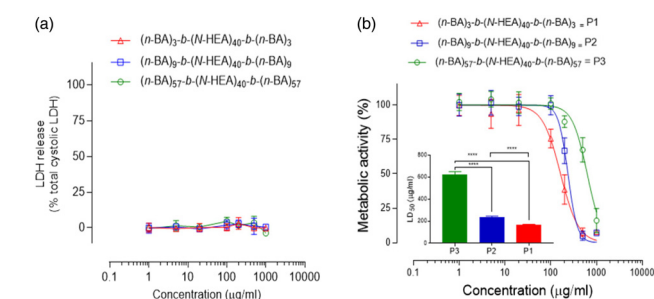

Fig. 9 Toxicity profiles of the synthesized (n-BA)$_m$-b-(N-HEA)$_{40}$-b-(n-BA)$_m$ copolymers. (a) Plasma membrane integrity of Calu-3 cells following 24 hour exposure to compounds determined by the LDH release assay. Data presented as mean ± SD, and represent triplicates from three independent experiments. (b) Metabolic activity of Calu-3 cells following 24 hour exposure to copolymers determined by the MTS assay. Data presented as mean ± SD and represent triplicate samples from three independent experiments. Statistical significance was determined by one-way ANOVA followed by Tukey's *post hoc* test (****, $p < 0.0001$).
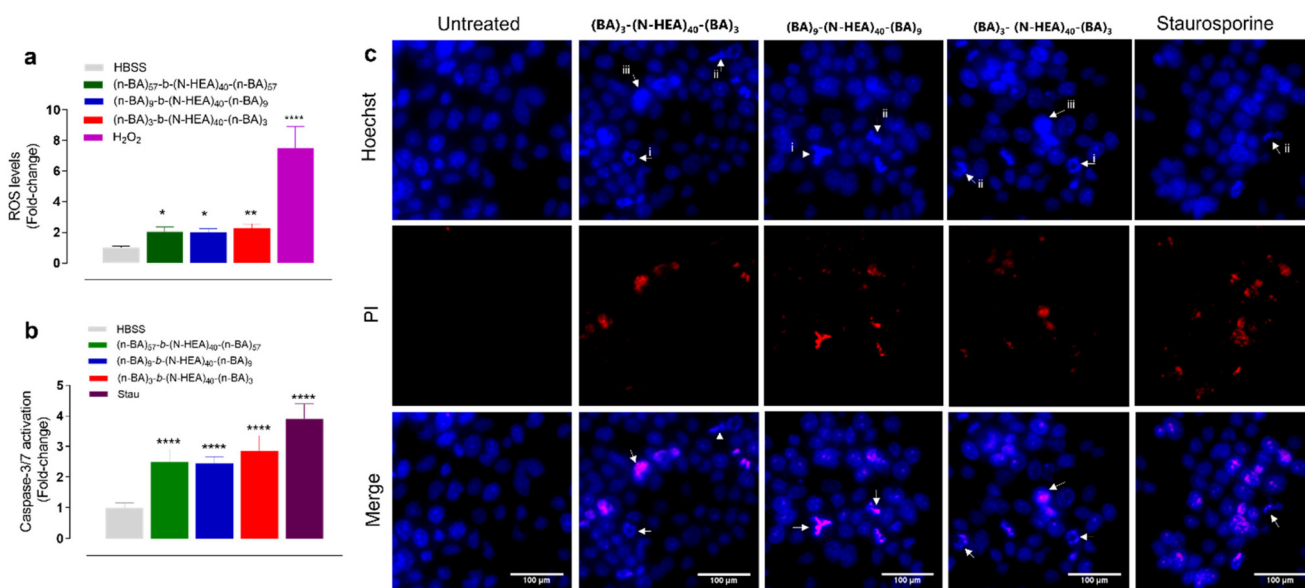

Fig. 10 Characteristic features of the synthesized (n-BA)$_m$-b-(N-HEA)$_{40}$-b-(n-BA)$_m$ toxicity on Calu-3 cells. (a) Intracellular ROS levels were assessed using the CM-H2DCFDA probe. H$_2$O$_2$ was used as the positive ROS-inducing control and applied at 1 mM. (b) Activation of pro-apoptotic caspase-3/7 was measured using the CellEvent probe. Staurosporine (Stau) was used as the positive apoptotic control and applied at 10 μM. (c) Images of Hoechst/propidium iodide (PI) staining of nuclei. White arrows indicate the presence of apoptotic features including (i) nuclear fragmentation, (ii) apoptotic bodies, and (iii) chromatin condensation. The scale bar is 100 μm. (a–c) Copolymers were incubated for 24 hours in a concentration with their LD$_{50}$ values. (a and b) Data presented as mean ± S.D (n = 3). Statistical significance was determined by one-way ANOVA followed by Tukey's *post hoc* test (*, $p < 0.05$; **, $p < 0.01$; ***, $p < 0.001$; ****, $p < 0.0001$).

values (shown as a bar chart in the inset) for $(n\text{-BA})_3\text{-}b\text{-}(N\text{-}HEA)_{40}\text{-}b\text{-}(n\text{-BA})_3$, $(n\text{-BA})_9\text{-}b\text{-}(N\text{-}HEA)_{40}\text{-}b\text{-}(n\text{-BA})_9$ and $(n\text{-BA})_{57}\text{-}b\text{-}(N\text{-}HEA)_{40}\text{-}b\text{-}(n\text{-BA})_{57}$ of 163.7 ± 6.9, 236.9 ± 8.0 and 625.2 ± 25.5 µg mL^{-1}, respectively, all of which differ significantly from each other ($p > 0.0001$), and indicate relatively low toxicity of the copolymers to epithelial cells.

The data hence indicate that a metabolic decline occurs in the absence of cell membrane damage. This suggests that the copolymers do not cause perturbations of the cell plasma membrane, as typically seen for amphipathic surfactants which damage the plasma membrane by the insertion of their hydrophobic moiety.[35] Thus, an alternative toxicity mechanism may have occurred.

We hence investigated a potential mechanism(s) of cell death induced by the copolymers by assessing cellular ROS generation, effector caspase-3/7 activation, and nuclear morphology and permeability (Fig. 10). The application of copolymers at concentrations above determined LD$_{50}$ (from Fig. 9) resulted in the significant generation of ROS, with all copolymers inducing ROS levels 2-fold greater than the untreated control (Fig. 10a). Moreover, at these concentrations, the copolymers generated significant levels of activated caspases-3/7, between 2 to 3-fold greater than untreated cells (Fig. 10b). Fluorescence microscopy imaging of Hoechst 33342 and PI-stained cells, presented in Fig. 10c, demonstrates that application of the copolymers above their LD$_{50}$ concentrations induces changes in nucleus morphology, observed *via* Hoechst staining, and results in increases in nuclear permeability, as indicated by positive PI staining. The nuclei of the treated cells exhibit signs of chromatid condensation, nuclear fragmentation, and the presence of apoptotic bodies, which are well-known pro-apoptotic features, and observed following exposure to all copolymers and the apoptotic control (staurosporine treatment). Furthermore, it was noted that positive PI nuclear staining was not observed in all cells treated with the copolymers or staurosporine, but predominately in those showing pro-apoptotic nuclear morphologies. Together, these data suggest that cells, under the conditions tested, underwent late apoptosis.

The toxicity at higher concentrations thus appears to arise from the initiation of cellular apoptosis, *i.e.*, by decreasing mitochondrial activity. In comparison, Pluronics®, poly(ethylene oxide)-*co*-poly(propylene oxide)-*co*-poly(ethylene oxide), a linear triblock copolymer, appears to exert its cytotoxic activity by interrupting cell membrane integrity and mitochondrial activity.[36,37] Considering the differences in chain composition and properties between $(n\text{-BA})_m\text{-}b\text{-}(N\text{-}HEA)_{40}\text{-}b\text{-}(n\text{-BA})_m$ and Pluronics®, including their 'opposite' block sequences, these all may contribute to the observed differences in the toxicity mechanism.

Conclusions

This study applies a combination of SET-LRP and photo-induced LRP techniques to synthesize block copolymers – $(n\text{-BA})_m\text{-}b\text{-}(N\text{-}HEA)_n\text{-}b\text{-}(n\text{-BA})_m$ – containing poly(N-hydroxyethyl acrylamide) as a water soluble middle A block, the structure that, to the best of our knowledge, has not been previously studied. NMR analysis of the copolymers in their common solvents (DMSO-d_6/acetone-d_6 mixture and MeOH-d_4) indicates the presence of partially solvated poly(n-butyl acrylate) blocks and a well-solvated poly(N-hydroxyethyl acrylamide) block in a DMSO-d_6/acetone-d_6 mixture, whilst in MeOH the presence of well-solvated $(n\text{-BA})_m$ B blocks is seen with partially solvated $(N\text{-}HEA)_{40}$ areas, inverse to the solvation in a DMSO-d_6/acetone-d_6 mixture.

This partial solvation of the constitutive blocks in the best common solvents, together with differences in the tested copolymer composition, *i.e.*, length of the B blocks, may contribute to the formation of self-assembled structures with varied morphologies and broad size distribution on the introduction of a miscible solvent (water) selective for the poly(N-hydroxyethyl acrylamide) block. It is interesting to note that despite their amphiphilic architecture, the copolymers do not cause appreciable damage to the cell membrane, typical of amphipathic materials, even on 24 hour exposure, and possess relatively high LD$_{50}$ in the range of 160–625 µg mL^{-1}. The toxicity mechanism observed upon cellular exposure to the copolymers at LD$_{50}$ concentrations involves apoptosis-mediated cell death. We envisage that the poly(N-hydroxyethyl acrylamide) block as the middle block in ABA copolymers can be further explored to, *via e.g.* 'click-chemistry', introduce different surface functionalities to the assemblies formed.

Conflicts of interest

There are no conflicts to declare.

References

1 N. P. Balsara, M. Tirrell and T. P. Lodge, Micelle Formation of BAB Triblock Copolymers in Solvents That Preferentially Dissolve the A Block, *Macromolecules*, 1991, **24**(8), 1975–1986, DOI: 10.1021/ma00008a040.

2 H. Wada, Y. Kitazawa, S. Kuroki, Y. Tezuka and T. Yamamoto, NMR Relaxometry for the Thermal Stability and Phase Transition Mechanism of Flower-like Micelles from Linear and Cyclic Amphiphilic Block Copolymers, *Langmuir*, 2015, **31**(32), 8739–8744, DOI: 10.1021/acs.langmuir.5b01902.

3 A. J. De Graaf, I. I. Azevedo Próspero Dos Santos, E. H. E. Pieters, D. T. S. Rijkers, C. F. Van Nostrum, T. Vermonden, R. J. Kok, W. E. Hennink and E. Mastrobattista, A Micelle-Shedding Thermosensitive Hydrogel as Sustained Release Formulation, *J. Controlled Release*, 2012, **162**(3), 582–590, DOI: 10.1016/j.jconrel.2012.08.010.

4 M. A. Moretton, C. Hocht, C. Taira and A. Sosnik, Rifampicin-Loaded 'Flower-like' Polymeric Micelles for

Enhanced Oral Bioavailability in an Extemporaneous Liquid Fixed-Dose Combination with Isoniazid, *Nanomedicine*, 2014, **9**(11), 1635–1650, DOI: **10.2217/nnm.13.154**.

5 C. Bruce, I. Javakhishvili, L. Fogelström, A. Carlmark, S. Hvilsted and E. Malmström, Well-Defined ABA- and BAB-Type Block Copolymers of PDMAEMA and PCL, *RSC Adv.*, 2014, **4**(49), 25809–25818, DOI: **10.1039/C4RA04325A**.

6 G. Bonacucina, M. Cespi, G. Mencarelli, G. Giorgioni and G. F. Palmieri, Thermosensitive Self-Assembling Block Copolymers as Drug Delivery Systems, *Polymer*, 2011, **3**(2), 779–811, DOI: **10.3390/polym3020779**.

7 M. Najafi, N. Kordalivand, M. A. Moradi, J. Van Den Dikkenberg, R. Fokkink, H. Friedrich, N. A. J. M. Sommerdijk, M. Hembury and T. Vermonden, Native Chemical Ligation for Cross-Linking of Flower-Like Micelles, *Biomacromolecules*, 2018, **19**(9), 3766–3775, DOI: **10.1021/acs.biomac.8b00908**.

8 F. Nederberg, Y. Zhang, J. P. K. Tan, K. Xu, H. Wang, C. Yang, S. Gao, X. D. Guo, K. Fukushima, L. Li, J. L. Hedrick and Y.-Y. Yang, Biodegradable Nanostructures with Selective Lysis of Microbial Membranes, *Nat. Chem.*, 2011, **3**(5), 409–414, DOI: **10.1038/nchem.1012**.

9 A. Simula, G. Nurumbetov, A. Anastasaki, P. Wilson and D. M. Haddleton, Synthesis and Reactivity of Homotelechelic Polymers by Cu(0)-Mediated Living Radical Polymerisation, *Eur. Polym. J.*, 2015, **62**, 294–303, DOI: **10.1016/j.eurpolymj.2014.07.014**.

10 Q. Zhang, P. Wilson, Z. Li, R. Mchale, J. Godfrey, A. Anastasaki, C. Waldron and D. M. Haddleton, Aqueous Copper-Mediated Living Polymerisation: Exploiting Rapid Disproportionation of CuBr with Me 6 TREN, *J. Am. Chem. Soc.*, 2013, **135**(19), 7355–7363 **https://pubmed.ncbi.nlm.nih.gov/23597244/**.

11 S. R. Samanta, H. Sun, A. Anastasaki, M. Haddleton and V. Percec, Self-activation and activation of Cu(0) wire for SET-LRP mediated by fluorinated alcohols, *Polym. Chem.*, 2014, **5**, 89–95 **https://pubs.rsc.org/en/content/articlelanding/2014/py/c3py01007d**.

12 A. Anastasaki, V. Nikolaou, A. Simula, J. Godfrey, M. Li, G. Nurumbetov, P. Wilson and D. M. Haddleton, Expanding the Scope of the Photoinduced Living Radical Polymerisation of Acrylates in the Presence of $CuBr_2$ and Me_6-Tren, *Macromolecules*, 2014, **47**(12), 3852–3859, DOI: **10.1021/ma500787d**.

13 A. Simula, V. Nikolaou, A. Anastasaki, F. Alsubaie, G. Nurumbetov, P. Wilson, K. Kempe and D. M. Haddleton, Synthesis of Well-Defined αalfa,omega-Telechelic Multiblock Copolymers in Aqueous Medium: In Situ Generation of α-Diols, *Polym. Chem.*, 2015, **6**(12), 2226–2233, DOI: **10.1039/C4PY01802H**.

14 C. MacDonald, W. Lyzenga, D. Shao and R. U. Agu, Water-Soluble Organic Solubilizers for in Vitro Drug Delivery Studies with Respiratory Epithelial Cells: Selection Based on Various Toxicity Indicators, *Drug Delivery*, 2010, **17**(6), 434–442, DOI: **10.3109/10717541003777548**.

15 G. Lligadas, B. M. Rosen, M. J. Monteiro and V. Percec, Solvent Choice Differentiates SET-LRP and Cu-Mediated Radical Polymerisation with Non-First-Order Kinetics, *Macromolecules*, 2008, **41**(22), 8360–8364, DOI: **10.1021/ma801774d**.

16 S. R. Samanta, H.-J. Sun, A. Anastasaki, D. M. Haddleton and V. Percec, Self-activation and activation of Cu(0) wire for SET-LRP mediated by fluorinated alcohols, *Polym. Chem.*, 2014, **5**, 89–95 **https://pubs.rsc.org/en/content/articlelanding/2014/py/c3py01007d**.

17 C. Boyer, A. H. Soeriyadi, B. Zetterlund and M. R. Whittaker, Synthesis of Complex Multiblock Copolymers via a Simple Iterative Cu(0)-Mediated Radical Polymerisation Approach, *Macromolecules*, 2011, **44**, 8028–8033, DOI: **10.1021/ma201529j**.

18 F. Nyström, A. H. Soeriyadi, C. Boyer, P. B. Zetterlund and M. R. Whittaker, End-Group Fidelity of Copper(0)-Meditated Radical Polymerisation at High Monomer Conversion: An ESI-MS Investigation, *J. Polym. Sci., Part A: Polym. Chem.*, 2011, **49**(24), 5313–5321, DOI: **10.1002/pola.25010**.

19 M. E. Levere, N. H. Nguyen and V. Percec, No Reduction of $CuBr_2$ during Cu(0)-Catalyzed Living Radical Polymerisation of Methyl Acrylate in DMSO at 25 °C, *Macromolecules*, 2012, **45**, 8267–8274, DOI: **10.1021/ma301547n**.

20 G. Lligadas and V. Percec, Synthesis of Perfectly Bifunctional Polyacrylates by Single-Electron-Transfer Living Radical Polymerisation, *J. Polym. Sci., Part A: Polym. Chem.*, 2007, **45**(20), 4684–4695, DOI: **10.1002/pola.22307**.

21 T. Hatano, B. M. Rosen and V. Percec, SET-LRP of Vinyl Chloride Initiated with CHBr3 and Catalyzed by Cu(0)-Wire/TREN in DMSO at 25 °C, *J. Polym. Sci., Part A: Polym. Chem.*, 2010, **48**(1), 164–172, DOI: **10.1002/pola.23774**.

22 X. Leng, N. H. Nguyen, B. van Beusekom, D. A. Wilson, V. Percec, M. E. Levere, D. A. Wilson, M. J. Monteiro and V. Percec, SET-LRP of 2-Hydroxyethyl Acrylate in Protic and Dipolar Aprotic Solvents, *Polym. Chem.*, 2013, **4**(10), 2995, DOI: **10.1039/c3py00048f**.

23 G. Lligadas and V. Percec, Ultrafast SET-LRP of Methyl Acrylate at 25 °C in Alcohols, *J. Polym. Sci., Part A: Polym. Chem.*, 2008, **46**(8), 2745–2754, DOI: **10.1002/pola.22607**.

24 N. H. Nguyen, J. Kulis, H.-J. Sun, Z. Jia, B. van Beusekom, M. E. Levere, D. A. Wilson, M. J. Monteiro, V. Percec, J. A. Yoon, S. S. Sheiko, S. Z. D. Cheng, A. Zhang, G. Ungar, D. J. P. Yeardley, B. M. Rosen, A. O. Argintaru, M. J. Sienkowska, K. Rissanen, S. Nummelin and J. Ropponen, A Comparative Study of the SET-LRP of Oligo(Ethylene Oxide) Methyl Ether Acrylate in DMSO and in H_2O, *Polym. Chem.*, 2013, **4**(1), 144–155, DOI: **10.1039/C2PY20782F**.

25 N. H. Nguyen, B. M. Rosen and V. Percec, SET-LRP of N,N-Dimethylacrylamide and of n-Isopropylacrylamide at 25 C in Protic and in Dipolar Aprotic Solvents, *J. Polym. Sci., Part A: Polym. Chem.*, 2010, **48**(8), 1752–1763, DOI: **10.1002/pola.23940**.

26 Y. Deng, J. Z. Zhang, Y. Li, J. Hu, D. Yang and X. Huang, Thermoresponsive Graphene Oxide-PNIPAM Nanocomposites with Controllable Grafting Polymer Chains via Moderate in Situ SET-LRP, *J. Polym. Sci., Part A: Polym. Chem.*, 2012, **50**(21), 4451–4458, DOI: **10.1002/pola.26259**.

27 *Introduction to Spectroscopy*, ed. D. L. Pavia, G. M. Lampman, G. S. Kriz and J. R. Vyvyan, Sengage Learning, 2015.

28 D. Neugebauer, B. S. Sumerlin, K. Matyjaszewski, B. Goodhart and S. S. Sheiko, How Dense Are Cylindrical Brushes Grafted from a Multifunctional Macroinitiator?, *Polymer*, 2004, **45**(24), 8173–8179, DOI: **10.1016/j.polymer.2004.09.069**.

29 C. Reichardt, Solvatochromic Dyes as Solvent Polarity Indicators, *Chem. Rev.*, 1994, **94**(8), 2319–2358.

30 J. E. Del Bene, S. A. Perera and R. J. Bartlett, Hydrogen Bond Types, Binding Energies, and ^{1}H NMR Chemical Shifts, *J. Phys. Chem. A*, 1999, **103**(40), 8121–8124, DOI: **10.1021/jp9920444**.

31 D. Fioretto, A. Livi, P. A. Rolla, G. Socino and L. Verdini, The Dynamics of Poly(n-Butyl Acrylate) above the Glass Transition, *J. Phys.: Condens. Matter*, 1994, **6**(28), 5295, DOI: **10.1088/0953-8984/6/28/007**.

32 J. L. de la Fuente, M. Fernández-García and E. López Madruga, Characterization and Thermal Properties of Poly (n-Butyl Acrylate-g-Styrene) Graft Copolymers, *J. Appl. Polym. Sci.*, 2001, **80**(5), 783–789, DOI: **10.1002/1097-4628(20010502)80:5<783::AID-APP1155>3.0.CO;2-5**.

33 C. Lang, J. A. LaNasa, N. Utomo, Y. Xu, M. J. Nelson, W. Song, M. A. Hickner, R. H. Colby, M. Kumar and R. J. Hickey, Solvent-Non-Solvent Rapid-Injection for Preparing Nanostructured Materials from Micelles to Hydrogels, *Nat. Commun.*, 2019, **10**(1), 3855, DOI: **10.1038/s41467-019-11804-7**.

34 R. C. Hayward and D. J. Pochan, Tailored Assemblies of Block Copolymers in Solution: It Is All about the Process, *Macromolecules*, 2010, **43**(8), 3577–3584, DOI: **10.1021/ma9026806**.

35 R. J. Cavanagh, P. A. Smith and S. Stolnik, Exposure to a Nonionic Surfactant Induces a Response Akin to Heat-Shock Apoptosis in Intestinal Epithelial Cells: Implications for Excipients Safety, *Mol. Pharm.*, 2019, **16**(2), 618–631, DOI: **10.1021/acs.molpharmaceut.8b00934**.

36 M. Redhead, G. Mantovani, S. Nawaz, P. Carbone, D. C. Gorecki, C. Alexander and C. Bosquillon, Relationship between the Affinity of PEO-PPO-PEO Block Copolymers for Biological Membranes and Their Cellular Effects, *Pharm. Res.*, 2012, **29**(7), 1908–1918, DOI: **10.1007/s11095-012-0716-6**.

37 G. Pembouong, N. Morellet, T. Kral, M. Hof, D. Scherman, M. F. Bureau and N. Mignet, A Comprehensive Study in Triblock Copolymer Membrane Interaction, *J. Controlled Release*, 2011, **151**(1), 57–64, DOI: **10.1016/j.jconrel.2011.01.007**.